On optimal capturing velocity of 2D rigid cylinder in general asymmetric v- shaped groove bracket and asymmetric wall friction

JACOB NAGLER
NIRC,
Haifa, Givat Downes
ISRAEL

Abstract: - The current paper calculates analytically the minimum required torque for cylinder movement together with the optimal (maximum) capturing velocity allowed to operate over a 2D rigid cylinder mass body that is placed inside a rigid general asymmetric shaped v-groove rigid bracket with asymmetric wall. The parametric analytic solution has been derived using generalized equations of motion – body-force derivations and kinematics alongside angular momentum equation for five cases scenarios: pure slip state, slip state that turn into rotational state, pure rotational state during the cylinder motion and the minimum required torque to initiate rotational movement and initial slip movement conditions, respectively. The motivation is to understand carrying devices better designing through cylindrical loading-bracket relationships.

Key-Words: cylinder, 2D rigid body, asymmetric v-groove, two-dimensional, capturing velocity, minimum torque, bracket, wall friction.

Received: May 9, 2024. Revised: October 9, 2024. Accepted: November 14, 2024. Published: December 27, 2024.

1 Introduction

The problem of captured mass - body between surfaces or walls with or without friction has many applications and importance in mechanical and civil engineering (rotary and linear positioning systems and high precision systems), as well. For instance, the importance of spinning friction in the context of bearing rolling balls on flat plates and in V-grooves was proved by Reichenbach [1] and later by Halling [2] in the 60s of the 20th century, respectively. However, whilst both studies investigate friction in ball bearings, yet, they focus on different aspects and use different approaches. Reichenbach [1] has investigated the sources of friction in thrust-carrying ball bearings using experimental tests to demonstrate that spinning of the balls is the primary contributor to friction, not internal material properties, especially for high-temperature applications. Halling [2] has analyzed contact conditions in angular-contact thrust ball bearings, proposing a new method considering elastic surface deformations to improve the accuracy of predicting frictional energy losses.

About two decades later, Hart [3] investigated analytically horizontal shafts supported by a V-grooved pulley wheel through modified Atwood machine analysis. He has found analytically the required pulley torque on the shaft when the pulley wheels are at rest or rotating counter to each other. Current problems will be analyzed analytically in a similar way including further generalization.

Another application of walls capturing mass-body was investigated by Dong et al. [4]. The researchers [4] delved into the critical issue of slip between the tool and workpiece in cross-wedge rolling process (CWR), a metal forming process used in tool design and product development. It employs a three-pronged approach: experimental, by validating a sophisticated computer model (FEM) of the CWR process, numerical simulations, by analyzing various CWR scenarios (14 in total) using the validated FEM to understand how factors like friction coefficient, forming angle, and area reduction influence slip, and analytically, by developing a formula to predict when the workpiece starts to rotate. Followed by confirming results they have found that increased slip occurs with lower friction, larger forming angles, and smaller area reduction. They identified critical friction coefficient (around 0.3), slip rate behavior and rotational criteria for optimizing CWR processes.

In 2008, generalized study concerning the frictional behavior during the initial phase (pre-rolling) of rolling element systems, like bearings – in the context of ball bearings inside V-grooved tracks was carried out by De Moerlooze and Al-Bender [5]. The study provides experimental data and validates a model for understanding pre-rolling friction behavior in rolling element systems, particularly the influence of normal load over the hysteresis behavior. Pre-rolling is defined as the period between starting and reaching steady rolling motion, while Hysteresis friction is defined as the Friction with a "loop" in the force-displacement curve. Based on the author's previous pre-rolling friction analytical model, they developed an experimental investigation process to measure friction force under different normal loads (force pressing the elements together) on a dedicated test setup with balls rolling in V-grooves, inputting the measured sliding friction coefficient and spin values into their model. A good confirmation between the model and empirical results was found (less than 16% error for low loads, 5% for high loads). Finally, they observed a slight increase in rolling friction coefficient and minimal change in the "curvature" of the hysteresis loop with increasing normal load.

Finally, the effect of belt friction over a cylinder mass body was investigated by Lubarda [6]. His study investigates belt friction before the point of gross slip (complete sliding) occurs. It focuses on Gradual slip variation, assuming that slip increases progressively from the "pull-end" to the "hold-end" of the belt as the pull force increases. The local pressure and friction forces exerted by the belt on the cylinder at various points within the contact area were determined analytically in closed formulations. Both flat and V-shaped belt types were considered. The findings of Lubarda study [6] includes non-proportional forces - the total pressure and friction forces are not proportional to each other and are not mutually orthogonal throughout the contact area, except in the case of complete gross slip, alongside the importance of considering pull and hold forces, coefficient of friction, and slip variation for accurate analysis. More applications and modelling appear in the book entitled "Friction Science and Technology" by Blau [7].

The current essay concentrates on an analytic dynamic problem of two – dimensional (2D) rigid cylinder mass body located inside rigid general asymmetric shaped v-groove bracket with asymmetric wall friction starting a sudden move. The optimal (maximum) velocity that keep the cylinder captured inside the V-groove area domain during its motion and the minimum required torque to start initial motion on one of the walls were determined using equations of motion – body-force equalities and kinematics alongside angular momentum equation based on five cases scenarios. The motivation of this study is to bring together different aspects of rotating pipes within a movable or static device to understand the friction mechanism and the behavior of the pipe – device bracket relationship for the benefit of designing mechanical robust devices.

2 Physical Model

Consider a 2D rigid shaft / cylinder element located inside a rigid wedge V-groove shaped bracket in the lateral direction as shown in Fig. 1. Suddenly, due to external effect (e.g. impact) five physical scenarios relating the cylinder – bracket relationships are likely to occur:

1. Pure slip state.
2. Slip state that turns into rotational state.
3. Pure rotational state.
4. Cylinder initial start of rotational motion.
5. Cylinder initial start of slip motion.

while the V-groove bracket (channel shape) is constant. The current essay discussion is limited to only cylinder motion and the appropriate maximum magnitude value the velocity permitted to have, such as the cylinder will not be released freely from the groove and leave its capturing area during its motion. Also, it considers the required minimum torque to start an initial rotational motion. The Cartesian coordinate axes x-y located at the right wall are the same for all cases. Note that the mathematical representation and solution of the left wall is the same. An example, is a carrier of shafts that are located in V-groove shaped channel and suddenly the carrier stops or crashed or climbing / driving on step bumper such as lateral impact is exerted in the lateral direction threatening to overthrow the shafts / pipes loadings from the carrier position in the V- shaped groove bracket.

3 Mathematical Model and discussion

In order to solve those cases three mathematical D-O-F vectored forces diagrams will be illustrated in Fig.2 (a) – (c) that corresponds to 1-5 cylinder (with radius R) – groove wall relationship cases, respectively. The forces mg, $f_{s,i}$, $f_{k,i}$, N_1, N_2, R, α, β, L_1, L_2 represent the earth gravitational force (m – represent the cylinder mass and g is the gravitational acceleration), the static and kinetic forces in the right and left walls, the acting right wall normal force over the cylinder, the acting left wall normal force over the cylinder, the cylinder radius, the right wall angle (α), the left wall angle (β), the right wall length, the left wall length, respectively. Also, the static and kinetic friction forces on both rigid walls fulfill $f_{s,i} = \mu_{s,i}N_i, f_{k,i} = \mu_{k,i}N_i, i = 1, 2$ where $\mu_{s,i}$ and $\mu_{k,i}$ represent the static and kinetic friction coefficients in both the right and the left wall, respectively. The direction of the cylinder after start of motion in the ascending direction is inferred from the study of Carvalho and Sampaio e Sousa [8].

3.1 *Pure slip state*:

In the current pure slip state without rotation (as appear in Fig. 2(a)), the cylinder disconnects the left wall and moves upward (ascending) along the right wall x – axis direction, hence, the equations of force in the x and y directions are:

$$\begin{cases} x: \; f_{k,1} - mgsin\alpha = m\ddot{x}_{slip} & (1.1) \\ y: \; N_1 = mgcos\alpha & (1.2) \end{cases} \quad (1)$$

where $\ddot{x}_{slip}$ denote the developed acceleration along the x – axis direction. Substituting $f_{k,1} = \mu_{k,1}mgcos\alpha$ into (1.1) leads to the following definition of the acceleration:

$$\ddot{x}_{slip} = g(\mu_{k,1}cos\alpha - sin\alpha) \quad (2)$$

Since in the end of the all the velocity fulfills $v_{x=L} = 0$, then based on the kinematic relation using (2), yields:

$$(v_{x=L})^2 = (v_{max,x=0})^2 + 2\ddot{x}_{slip}L_1 = 0 \quad (3)$$

Accordingly, the extracted maximum velocity from (3) is:

$$v_{max,x=0} = 2g(sin\alpha - \mu_{k,1}cos\alpha)L_1 \quad (4)$$

Unsurprisingly, the maximum velocity linearly increases with the length wall L_1 and decreases with the kinematic viscosity $\mu_{k,1}$.

3.2 *Slip state with spinning that turn into rotational state*:

In this case, as appear in Fig. 2(b), the ascending cylinder with initial spinning angular velocity ω_0 climbs with unknown velocity $v_{max,x=0}$ and appropriate acceleration as expressed in (2) such as the kinematic relation supplies:

$$(v_{x=x_1})^2 = (v_{max,x=0})^2 + 2\ddot{x}_{slip}x_{1,slip} = (\omega R)^2 \quad (5)$$

where $x_{1,slip}$ is the slip cylinder body travel distance $x_{1,slip}$ and ω is the rotational angular velocity, while the full expression of the angular velocity fulfills:

$$\omega = \omega_0 - \alpha t, \;\; 0 \leq t \leq t_{slip} \quad (6)$$

whereas α is the rotational angular acceleration, t denotes the time increment.

Now, during climbing ascending, the friction moment is opposed to the rotational movement in order to decrease it. Accordingly, based on the analog Newton's rotational second law, we get the expression for α:

$$f_{k,1}R = I\alpha \rightarrow \alpha = \frac{f_{k,1}R}{I} = \frac{\mu_{k,1}\ N_{k,1}R}{I} = \mu_{k,1}\frac{mgR}{I}cos\alpha \quad (7)$$

Therefore Eq. (6) becomes after multiplying both sides by R and substituting (7) into (6):

$$v(t)_{rotational} = \omega R = \omega_0 R - \mu_{k,1}\frac{mgR^2cos\alpha}{I}\ t\ ,\ 0 \le t \le t_{slip} \quad (8)$$

In the same manner, we know that $v(t)_{slip}$ fulfills:

$$v(t)_{slip} = v_{max,x=0} + \ddot{x}_{slip}\ t,\ \ t_0 \le t \le t_{slip}, t_0 = 0 \quad (9)$$

Equating both expressions (8) – (9), gives the time of slip movement until it becomes rotational movement:

$$t_{slip} = \frac{\omega_0 R - v_{max,x=0}}{g(\mu_{k,1}cos\alpha - sin\alpha) + \mu_{k,1}\frac{mgR^2cos\alpha}{I}} \quad (10)$$

We will write (10) in the following convenient manner:

$$t_{slip} = \frac{\omega_0 R - v_{max,x=0}}{Q} \quad (11)$$

where $Q = g(\mu_{k,1}cos\alpha - sin\alpha) + \mu_{k,1}\frac{mgR^2cos\alpha}{I}$. Substituting (11) into the following kinematic relation, leads to the appropriate distance $x_{1,slip}$ expression that equals to:

$$x_{1,slip} = v_{max,x=0}t_{slip} + \frac{1}{2}\ddot{x}_{slip}t_{slip}^2 = v_{max,x=0}\frac{\omega_0 R - v_{max,x=0}}{Q} + \frac{1}{2}g(\mu_{k,1}cos\alpha - sin\alpha)\left(\frac{\omega_0 R - v_{max,x=0}}{Q}\right)^2 \quad (12)$$

Now, the relation for the pure rotational acceleration is:

$$\ddot{x}_{rotational} = -\alpha R = -\mu_{k,1}\frac{mgR^2}{I}cos\alpha \quad (13)$$

Hence, when the capturing velocity becomes zero at the V-shaped end: $v_{x=L} = 0$, the rotational kinematic relation:

$$(v_{x=L})^2 = \left(v_{rotational,x=x_1}\right)^2 + 2\ddot{x}_{rotational}(L_1 - x_{1,slip}) = 0 \quad (14)$$

Inserting (12)-(13) into (14), Eq. (14) becomes:

$$\left(\omega_0 R - \mu_{k,1}\frac{mgR^2cos\alpha}{I}\ \frac{\omega_0 R - v_{max,x=0}}{Q}\right)^2 = 2\mu_{k,1}\frac{mgR^2}{I}cos\alpha\left[L_1 - v_{max,x=0}\frac{\omega_0 R - v_{max,x=0}}{Q} - \frac{1}{2}g(\mu_{k,1}cos\alpha - sin\alpha)\left(\frac{\omega_0 R - v_{max,x=0}}{Q}\right)^2\right] \quad (15)$$

By defining that $Q_1 = \mu_{k,1}\frac{mgR^2cos\alpha}{I}$, Eq. (15) is simplified to:

$$\left[\omega_0 R - \frac{Q_1}{Q}\left(\omega_0 R - v_{max,x=0}\right)\right]^2 = 2Q_1\left[L_1 - v_{max,x=0}\frac{\omega_0 R - v_{max,x=0}}{Q} - \left(\frac{Q - Q_1}{2}\right)\left(\frac{\omega_0 R - v_{max,x=0}}{Q}\right)^2\right] \quad (16)$$

Accordingly, the obtained expression for the maximum capturing velocity dependent on ω_0 is:

$$v_{max,x=0} = \frac{Q_1\omega_0 R + \sqrt{QQ_1(\omega_0 R)^2 - 2L_1 QQ_1^2}}{Q_1} = \omega_0 R + Q^2\sqrt{\frac{(\omega_0 R)^2}{Q_1} - 2L_1} \quad (17)$$

By substituting back Q and Q_1 relations into (17) we get:

$$v_{max,x=0} = \omega_0 R + \sqrt{\frac{(\mu_{k,1}mR^2 + \mu_{k,1}I - Itan\alpha)(-2L_1 g\mu_{k,1}mcos\alpha + I\omega_0^2)}{\mu_{k,1}Im}} \quad (18)$$

Observation on Eq. (18) leads to understanding that the maximum capturing velocity increases with the initial spinning velocity ω_0 and the geometric radius R and decreases with the kinematic viscosity increase $\mu_{k,1}$. Validation of the previous analytic expression for $v_{max,x=0}$ has been achieved by using the following kinematic relation:

$$\left(v_{max,x=0}\right)^2 + 2\ddot{x}_{slip}x_{1,slip} = \left(v_{rotational,x=x_1}\right)^2 \quad (19)$$

3.3 *Pure rotational state*:

In this case, as appear in Fig. 2(c), the ascending cylinder climbs with unknown velocity $v_{max,x=0}$ and appropriate acceleration as expressed in (13), adding the end condition $v_{x=L} = 0$ into the following kinetic relation, simply yields:

$$(v_{x=L})^2 = \left(v_{max,x=0}\right)^2 + 2\ddot{x}_{rotational}L_1 = 0 \quad (20)$$

Following the substituting of (13) into (20), yields:

$$v_{max,x=0} = R\sqrt{2\mu_{k,1}\frac{mgL_1}{I}cos\alpha} \quad (21)$$

Observations at Eq. (21) show that the maximum capturing velocity increases with the cylinder radius (R) as well with the wall length (L_1) and the cylinder mass (m) increase, respectively. Although it decreases with the second moment of inertia (I). The logic behind the results is due to the fact that the ascending moment decrease due to the counter friction moment that depends on those mentioned parameters ($\sim\mu_{k,1}mgcos\alpha$) then the required kinetic energy should increase.

3.4 *Cylinder initial start of rotational motion*:

Generalizing Hart [3] analysis, meaning, what should be the minimum torque value (T_{min}) to fulfill the required initial start of rotational motion , hence, the following body forces equations act on the cylinder in the x-y Cartesian axes directions appearing in Fig. 2(d) are:

$$\begin{cases} x: F_{s,1} - mgsin\alpha + N_2(sin\beta cos\alpha + sin\alpha cos\beta) + \\ \quad F_{s,2}(cos\beta cos\alpha - sin\beta sin\alpha) = m\ddot{\theta}R \ (22.1) \\ y: \quad N_1 - mgcos\alpha + N_2(cos\beta cos\alpha - sin\beta sin\alpha) \\ \quad -F_{s,2}(cos\beta sin\alpha + sin\beta cos\alpha) = 0 \ (22.2) \end{cases} \quad (22)$$

The angular momentum equation of the cylinder is:

$$F_{s,1}R + F_{s,2}R = I\ddot{\theta} \quad (23)$$

By substituting the relations $F_{s,1} = \mu_{s,1}N_1$ and $F_{s,2} = \mu_{s,2}N_2$ into (22) – (23) leads to the following equations system:

$$\begin{cases} x: \mu_{s,1}N_1 - mgsin\alpha + N_2(sin\beta cos\alpha + sin\alpha cos\beta) + \\ \quad \mu_{s,2}N_2(cos\beta cos\alpha - sin\beta sin\alpha) = m\ddot{\theta}R \ (24.1) \\ y: \quad N_1 - mgcos\alpha + N_2(cos\beta cos\alpha - sin\beta sin\alpha) \\ \quad -\mu_{s,2}N_2(cos\beta sin\alpha + sin\beta cos\alpha) = 0 \ (24.2) \end{cases} \quad (24)$$

The angular momentum equation of the cylinder is:

$$\mu_{s,1}N_1R + \mu_{s,2}N_2R = I\ddot{\theta} = T_{min} \quad (25)$$

By substituting (25) into (24.1) equilibrium we can easily find expression of the unknown constants N_1, N_2 as:

$$\begin{cases} N_1 = D_2 + \frac{[D_2\mu_{S,1}(C_1-1)+D_1](\mu_{S,2}B_2-A_2)}{A_2\mu_{S,1}(C_1-1)-B_2\mu_{S,1}\mu_{S,2}(C_1-1)+\mu_{S,2}(B_1-C_1)+A_1} \\ N_2 = \frac{D_2\mu_{S,1}(C_1-1)+D_1}{A_2\mu_{S,1}(C_1-1)-B_2\mu_{S,1}\mu_{S,2}(C_1-1)+\mu_{S,2}(B_1-C_1)+A_1} \end{cases} \quad (26)$$

where $D_1 = mgsin\alpha, A_1 = sin\beta cos\alpha + sin\alpha cos\beta, B_1 = cos\beta cos\alpha - sin\beta sin\alpha, C_1 = \frac{mR^2}{I}$,
$D_2 = mgcos\alpha, A_2 = cos\beta cos\alpha - sin\beta sin\alpha, B_2 = cos\beta sin\alpha + sin\beta cos\alpha.$

3.5 *Cylinder initial start of slip motion*:

In this case, only alip mechanism is performed, such as system of Eq. (22) will be written as:

$$\begin{cases} x: \quad F_{k,1} - mgsin\alpha + N_2(sin\beta cos\alpha + sin\alpha cos\beta) + \\ \quad F_{k,2}(cos\beta cos\alpha - sin\beta sin\alpha) > 0 \ (27.1) \\ y: \quad N_1 - mgcos\alpha + N_2(cos\beta cos\alpha - sin\beta sin\alpha) - \\ \quad F_{k,2}(cos\beta sin\alpha + sin\beta cos\alpha) = 0 \ (27.2) \end{cases} \quad (27)$$

while the condition to start slip motion is simply that $N_2 = 0$ such as the cylinder disconnects from / relieves the right wall, accordingly:

$$F_{k,1} = \mu_{k,1}mgcos\alpha > mgsin\alpha \rightarrow tan\alpha < \mu_{k,1} \quad (28)$$

In general, the cross section's resistance to rotation is significant, the more sides there are the shape created from the circle has the greatest rotational potential with minimum energetic resistance to its rotation, while the resistance of a triangle is higher than a square, pentagon, hexagon, and so on as appear in Fig. 3*a-e*. It is important to note that the ratio of the lengths of the sides in a polygon also has a significant effect on the resistance to the section, the higher the base of the polygon is in a non-equilateral polygon, then its resistance to the rotational section increases.

4 Conclusion

To sum it up, the current essay contributes to understanding the issue of carrying devices of cylindrical loading and its relationship with its V-shaped groove bracket through friction understanding. A 2D rigid general cylinder element located inside rigid wedge V-groove shaped channel was considered. Suddenly, due to external effects (e.g. impact) five physical possible scenarios relating the cylinder – channel relationships were investigated: (i) Pure slip state. (ii) Slip state that turns into rotational state. (iii) Pure rotational state. (v) Cylinder initial start of rotational motion. (iv) Cylinder initial start of slip motion. A general parametric kinematic and body-forces model was proposed with appropriate analytic solutions.

References

[1] Reichenbach, G. S., (1960) The Importance of Spinning Friction in Thrust-Carrying Ball Bearings, *J. Basic Eng*. **82** (2) 295-300. DOI: 10.1115/1.3662578

[2] Hailing J. (1966) Second Paper: Analysis of Spin/Roll Conditions and the Frictional-Energy Dissipation in Angular-Contact Thrust Ball Bearings, *Proceedings of the Institution of Mechanical Engineers*. **181** (1) 349-362. DOI:10.1243/PIME_PROC_1966_181_035_02

[3] Hart, J. B., (1982) Frictional force rotator. *Am. J. Phys.* **50** (7) 631–634. DOI: 10.1119/1.13061

[4] Dong, Y., Tagavi, K. H., and Lovell, M. R., (2000) Analysis of interfacial slip in cross-wedge rolling: a numerical and phenomenological investigation, *JMPT* **97** (1–3) 44-53. DOI: 10.1016/S0924-0136(99)00285-X

[5] De Moerlooze, G., Al-Bender, F., (2007) Experimental Investigation into the Tractive Prerolling Behavior of Balls in V-Grooved Tracks, *Advances in Tribology*, Article ID 561280, 1-10. DOI: 10.1155/2008/561280

[6] Lubarda, V. A., (2015) Determination of the belt force before the gross slip, *Mechanism and Machine Theory* **83** 31–37.DOI: 0.1016/j.mechmachtheory.2014.08.015

[7] Blau, P. J., (2008) *Friction Science and Technology: from concepts to applications* 2nd ed., CRC Press: Taylor & Francis Group, Boca Raton, FL. https://www.routledge.com/Friction-Science-and-Technology-From-Concepts-to-Applications-Second-Edition/Blau/p/book/9780367386665

[8] Carvalho, P. S. and Sampaio e Sousa, A. 2005, Rotation in secondary school: teaching the effects of frictional force. *Phys. Educ*. **40** (3) 257 – 265.DOI: 10.1088/0031-120/40/3/007

Contribution of Individual Authors to the Creation of a Scientific Article (Ghostwriting Policy)

The author contributed in the present research, at all stages from the formulation of the problem to the final findings and solution.

Sources of Funding for Research Presented in a Scientific Article or Scientific Article Itself

No funding was received for conducting this study.

Conflict of Interest

The author has no conflict of interest to declare that is relevant to the content of this article.

APPENDIX

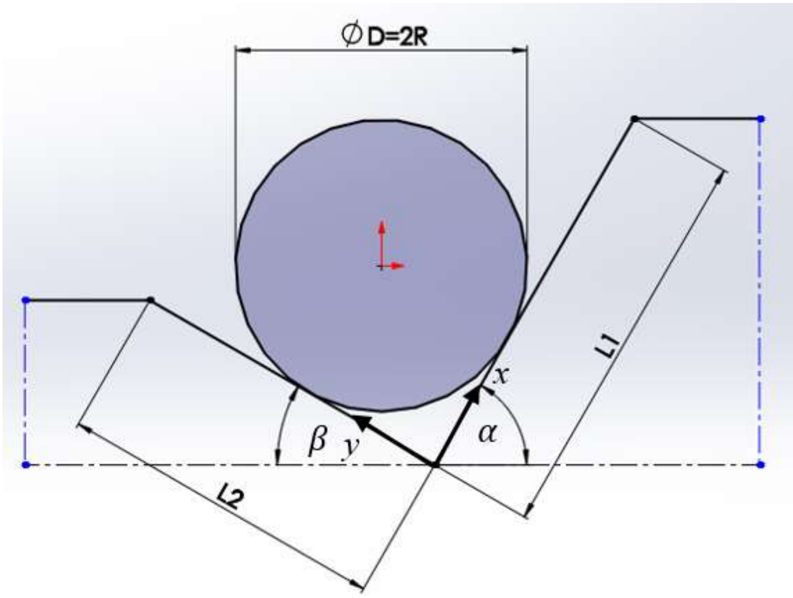

Fig. 1 2D lateral section of cylinder inside V- shaped asymmetric groove

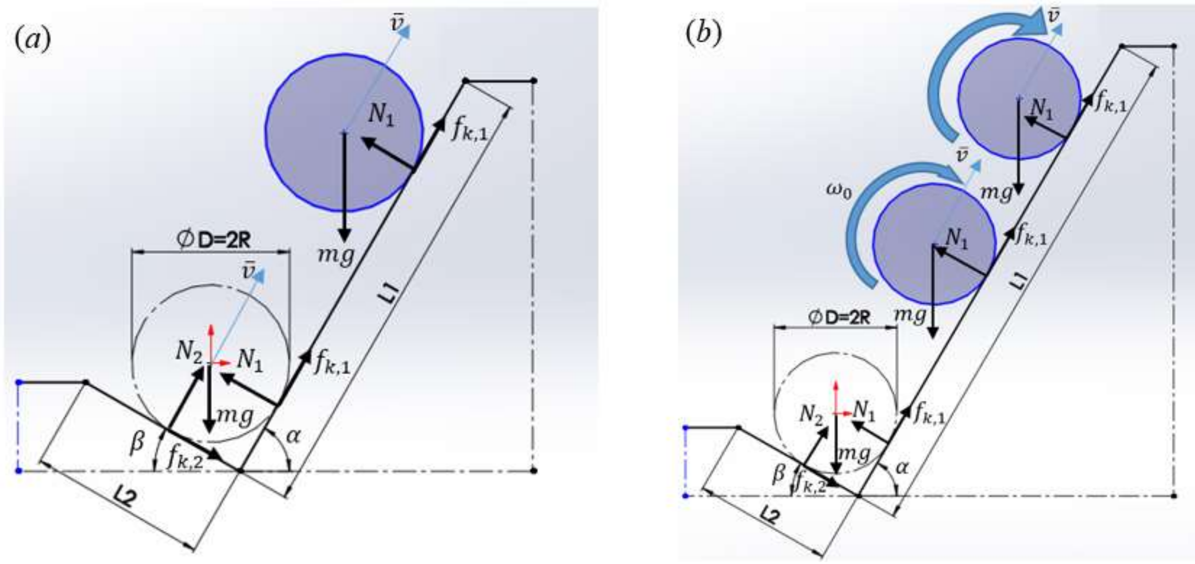

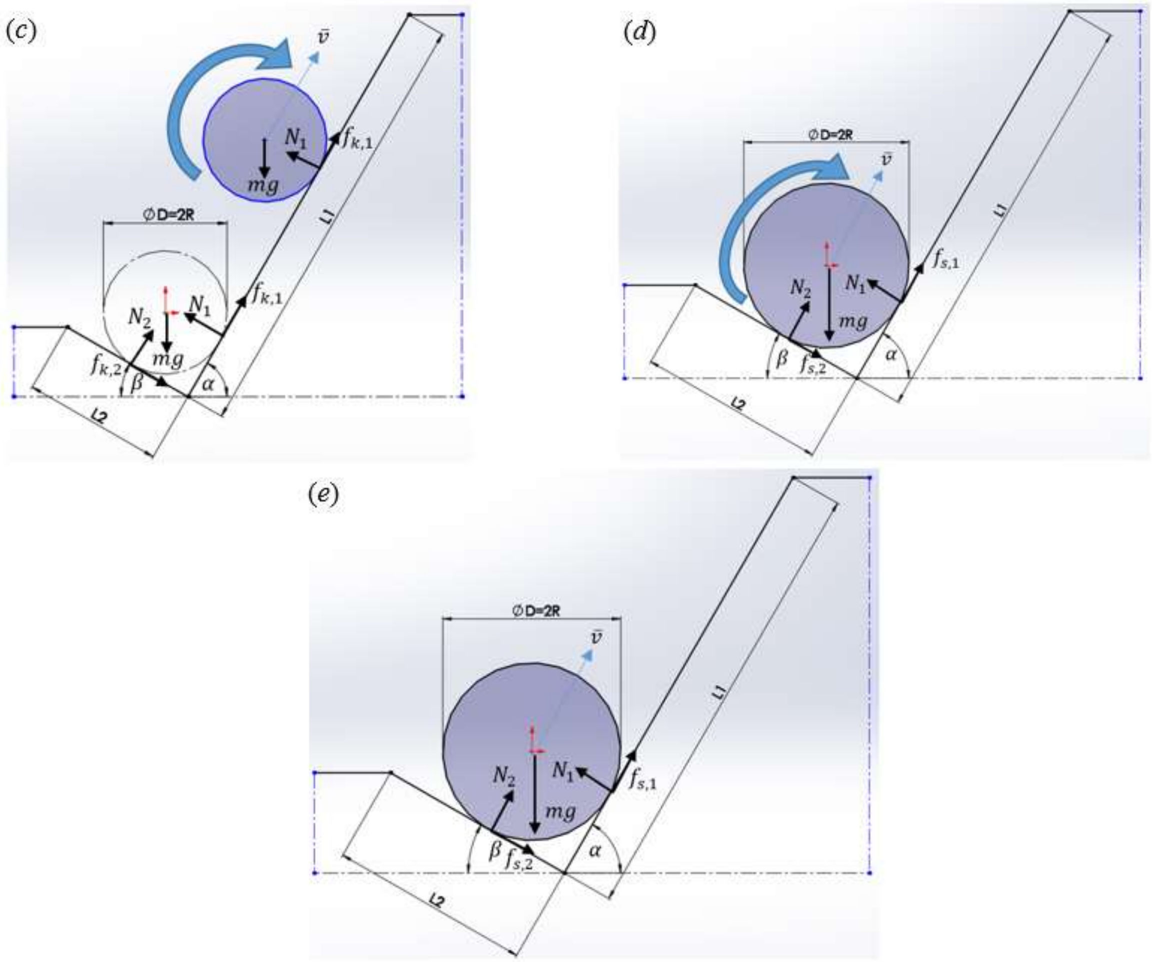

Fig. 2 (a) Pure slip state after start of motion (b) Slip state that turn into rotation state after start of motion (c) Pure rotational state after start of motion (d) Cylinder initial start of rotational motion (e) Cylinder initial start of slip motion

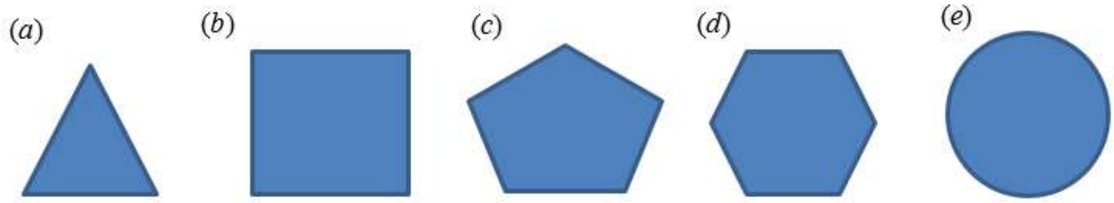

Fig. 3 Step-by-step images of cross-sections used for moment of inertia resisting modelling: (a) Triangle (b) Rectangular (c) Pentagon (d) Hexagon (e) Circular